



Colloidal Co nanoparticles supported on SiO₂: Synthesis, characterization and catalytic properties for steam reforming of ethanol

Renata U. Ribeiro ^a, Janete W.C. Liberatori ^a, Herbert Winnishofer ^{b,1},
José Maria C. Bueno ^a, Daniela Zanchet ^{b,*}

^a DEQ, Universidade Federal de São Carlos, C.P. 676, 13565-905 São Carlos, SP, Brazil

^b Laboratório Nacional de Luz Síncrotron – LNLS, C.P. 6192, 13083-970 Campinas, SP, Brazil

ARTICLE INFO

Article history:

Received 3 March 2009

Received in revised form 10 July 2009

Accepted 13 July 2009

Available online 18 July 2009

Keywords:

Cobalt

Nanoparticles

Steam reforming of ethanol

ABSTRACT

Colloidal Co nanoparticles with sizes in the 3–8 nm range were obtained by thermal decomposition of Co₂(CO)₈ in the presence of ligands and impregnated on SiO₂ to prepare SiO₂-supported Co nanocatalysts. The catalysts showed activity for the steam reforming of ethanol with higher values for smaller Co particles. H₂ adsorption results and Fourier transform infrared spectroscopy of adsorbed CO suggested that the fraction of accessible Co sites also depended on the synthesis conditions. Precipitation of the Co nanoparticles with methanol instead of ethanol before impregnation had a positive effect on the density of accessible Co sites to catalysis; similar result was verified by increasing the thermal treatment temperature under H₂ flow before the reaction. Based on the distribution of products with temperature of reaction, a mechanism for steam reforming of ethanol on SiO₂-supported Co nanocatalysts is suggested.

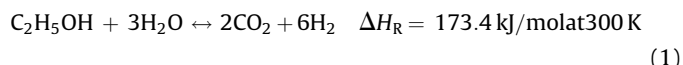
© 2009 Elsevier B.V. All rights reserved.

1. Introduction

Nanostructured materials usually present unique properties when compared to bulk, and understanding these materials has led to the development of new technologies in several fields, from nanoelectronics to catalysis [1]. Due to quantum confinement and surface effects, the properties of nanostructured materials depend on size and shape [2,3]. As a consequence, new routes to produce nanostructured materials in a controllable way have been pursuing as well as the development of advanced characterization tools required to understand and correlate nanoparticle size, shape and atomic distribution to macroscopic properties [4,5]. In catalysis, despite being a mature field, nanoscience and nanotechnology have already brought important contributions and much more is expected in a near future [1,6]. In particular, this approach should have an important impact in areas related to environment and production of clean energy, such as hydrogen based technologies. For example, supported catalysts are complex materials usually formed by metallic or oxide nanoparticles highly dispersed on supports, such as Al₂O₃ and SiO₂ among others. The rational exploitation of nanoscience in the design of model catalysts, where size dependent properties can be controlled systematically, may

speed up the development of new catalysts with enhanced performance. Elegant examples are already found in the literature, such as the use of colloidal Pt nanoparticles to address the size and shape dependence in Suzuki reactions [7] and the production of high-surface area catalysts [8]. The number of works exploiting this strategy has impressively increased in the last years [1,9–11].

One of the most demanding areas that require the development of high performance catalysts is the production of clean fuels, such as hydrogen. Hydrogen is an attractive alternative energy carrier but currently, it is still mostly produced by steam reforming of natural gas. The steam reforming of ethanol represents a strategic reaction to produce hydrogen from renewable sources (Eq. (1)). However, a complex reaction network can take place, depending on the reaction conditions and catalyst, as addressed in recent studies [12,13].



Cobalt catalysts are commonly used in steam reforming of ethanol due to the low cost and high activity for hydrogen production [14,15]. For example, a positive effect of cobalt addition to several oxides was shown by Llorca et al. [16]. Concerning the characteristics of the catalyst, Haga et al. [17] observed that the selectivity for steam reforming was closely related to the cobalt crystallite size, which depended on the cobalt precursor. Similar results were found by Song et al. [18], using a broader set of

* Corresponding author. Tel.: +55 19 3512 1049; fax: +55 19 3512 1004.

E-mail address: zanchet@lnls.br (D. Zanchet).

¹ Present address: Universidade Federal do Paraná, Curitiba, PR, Brazil.

supports. Other works also reported the influence of the preparation method in the product distribution for steam reforming [19,20], such as the choice of the cobalt precursor in Co/ZnO catalysts that directly affected the catalytic activity. Recently, Song and Ozkan [21] explored ZrO₂ and CeO₂ as supports to address the effect of oxygen mobility. Therefore, the method applied in the synthesis of catalysts can lead to materials with different properties and the understanding of the several critical parameters is still desirable.

In this work, we addressed the use of colloidal Co nanoparticles (Co-NPs) with different sizes (3–8 nm range) supported on SiO₂ (Co-NPs/SiO₂) in steam reforming of ethanol. The Co-NPs were obtained by thermal decomposition of Co₂(CO)₈ in the presence of ligands and solvent [22] and impregnated on silica. We investigated the influence of ligand/Co₂(CO)₈ molar ratio used in the synthesis of the Co-NPs, which determined the final particle size, the choice of the solvent used to precipitate the Co-NPs, and the temperature of activation of the Co-NPs/SiO₂ catalysts. To investigate the properties of Co-NPs and Co-NPs/SiO₂ catalysts the samples were characterized by X-ray diffraction (XRD), transmission electron microscopy (TEM), Fourier transform infrared spectroscopy (FTIR) of adsorbed CO, and FTIR during activation. The catalytic properties of Co-NPs/SiO₂ catalysts with temperature of reaction were investigated for hydrogenolysis of ethanol and for steam reforming of ethanol. A mechanism for steam reforming of ethanol on Co-NPs/SiO₂ catalysts is suggested.

2. Experimental

2.1. Catalyst preparation

The following reactants were used to produce colloidal Co-NPs: dicobalt octacarbonyl (Co₂(CO)₈) (Alfa Aesar), anhydrous 1,2-dichlorobenzene (C₆H₄Cl₂) (Aldrich), oleic acid (OA) (Acros Organic), tryoctylphosphine oxide (TOPO) (Alfa Aesar), methanol (Merck), ethanol (J. T. Baker), and octane and octanol (Merck).

Co-NPs were synthesized as described by Puentes et al. [22]. Briefly, Co₂(CO)₈ (1.6 mmol) was decomposed at high temperature (454 K) in anhydrous 1,2-dichlorobenzene in the presence of the surfactants oleic acid (OA) and tryoctylphosphine oxide (TOPO). While TOPO (0.25 mmol) was used to improve Co-NPs size distribution the OA/Co₂(CO)₈ molar ratio was varied (0.2, 0.4 and 0.8) to control the average Co-NP size. The reaction was carried out under inert atmosphere (Ar). In this work, the Co-NPs were precipitated with either ethanol or methanol. A mixture of 95% octane, 5% octanol and 1% OA was used to readily re-disperse the Co-NPs.

The silica-supported Co-NPs catalysts, Co-NPs/SiO₂, were obtained by impregnation of the colloidal Co-NPs on silica Cab-O-Sil L-90, with surface area of 87 m²/g. Three milliliter of colloidal suspension containing 10 mg of Co-NPs was sonicated for a few minutes in ultrasound and slowly added to 1 g of silica, obtaining a dark gel. This procedure was done inside a dry-box. After drying for 8 h, the Co-NPs/SiO₂ catalysts showed dark grey color and brittle texture, and were kept in inert atmosphere before being used. The silica-supported Co-NPs catalysts were labeled as *y*Co-NPs-*z*/SiO₂, where *y* is approximately the mean Co-NP size and *z* refers to methanol (MeOH) or ethanol (EtOH) used to precipitate the Co-NPs.

2.2. Characterization

Chemical analyses of the Co-NPs/SiO₂ catalysts were performed by atomic absorption spectrometry on an AA INTRALAB 1475 – EAA equipment.

Surface areas (*S*_{BET}) of SiO₂ and catalysts were measured by N₂ adsorption at 77 K using a QuantaChrome Nova 1200 apparatus.

XRD patterns of the colloidal Co-NPs were measured at the D10A-XRD2 beamline at the Brazilian Synchrotron Light Laboratory (LNLS), Campinas-SP, Brazil. The powder sample (after precipitation) was spread on a mis-cut Si wafer and covered with a small amount of oleic acid to avoid oxidation. The step-scans were collected within the 2θ range from 35° to 60° using λ = 1.62 Å (with step-sizes of 0.05°).

TEM images of Co-NPs and Co-NPs/SiO₂ catalysts were obtained in a JEOL JEM-3010 microscope (300 kV, 1.7 Å point resolution) at the LNLS, Campinas-SP, Brazil. TEM samples of Co-NPs were prepared by diluting the colloidal dispersion in hexane and dropping it onto amorphous carbon film supported on copper grid. In the case of the catalysts, the powder was suspended in isopropanol.

Hydrogen chemisorption experiments on Co-NPs/SiO₂ catalysts were performed in a QuantaChrome Instrument Autosorb – 1-C. Prior to the adsorption, the samples were activated *in situ* under 50 ml/min H₂ flow following the steps: 2 K/min up to 373 K, holding time 0.5 h; 2 K/min up to 473 K, holding time 1 h and 10 K/min up to 623 K, holding time 2 h. The system was evacuated for 0.5 h at this temperature and cooled down at 5 K/min. Hydrogen chemisorption was then carried out at 323 K.

FTIR spectra were recorded using a Thermo Nicolet 4700 Nexus FT-IR spectrophotometer with MCT detector and diffuse reflectance infrared Fourier transform spectroscopy-reactor cell (Spectra Tech) with CaF₂ windows (DRIFTS HTHV cell). The activation of the undiluted Co-NPs/SiO₂ catalysts using H₂/N₂ (27/73, v/v) was performed similarly to the hydrogen chemisorption experiments. After each step, the sample was cooled to 298 K under H₂/N₂ flow (1:3) at 40 ml/min and the spectrum was collected under 40 ml/min of N₂ flow (64 scans, 4 cm⁻¹ resolution). Activation at 773 K was also performed. In this case, the sample was heated at 2 K/min and held for 3 h at 773 K.

Co-NPs/SiO₂ catalysts activated at 623 or 773 K were used in the FTIR of adsorbed CO experiments, which were carried out according to the method described in Ref. [23]. Briefly, the undiluted Co-NPs/SiO₂ catalysts were reduced in H₂/N₂ (27/73, v/v) by heating to 623 or 773 K at 5 K/min and holding for 2 h under a total flow of 25 ml/min. The samples were cooled to 298 K in H₂/N₂ flow and the DRIFTS cell was purged with dry N₂ free of O₂ for 15 min. The adsorption of CO was performed at 298 K with CO pulses (0.5 mL) at CO pressure of 20 Torr. Each spectrum was collected 5 min after each pulse in order to achieve equilibrium.

2.3. Catalytic reactions

The behavior of the catalysts in the hydrogenolysis of ethanol and their catalytic performances in the steam reforming of ethanol were evaluated in a fixed bed quartz reactor (i.d. 8 mm) operating isothermally at atmospheric pressure. The catalyst bed (160 mg) was maintained without temperature gradient across it. Prior the reactions, the samples were activated *in situ* with 50 ml/min H₂ flow, similar to the hydrogen chemisorption experiments. The hydrogenolysis of ethanol was carried out from 523 to 873 K, at atmospheric pressure, with a feed mixture of the 3:1 molar ratio of H₂/ethanol and a total liquid flow rate of 2 mL/h (WHSV for ethanol = 9.9 h⁻¹). The selectivity for steam reforming of ethanol was measured in the same temperature range and atmospheric pressure. The reaction mixture was 6:1 molar ratio of H₂O:ethanol with total liquid flow rate of 2 mL/h and 30 ml/min of He flow (WHSV for ethanol = 3.5 h⁻¹). The fractional distance from equilibrium (1 – η) in these experiments varied from 0.72 to 0.99. Net turnover rates (TOF_n) were used to obtain forward turnover rate (TOF_f) of the dehydrogenation reaction of ethanol, which is the

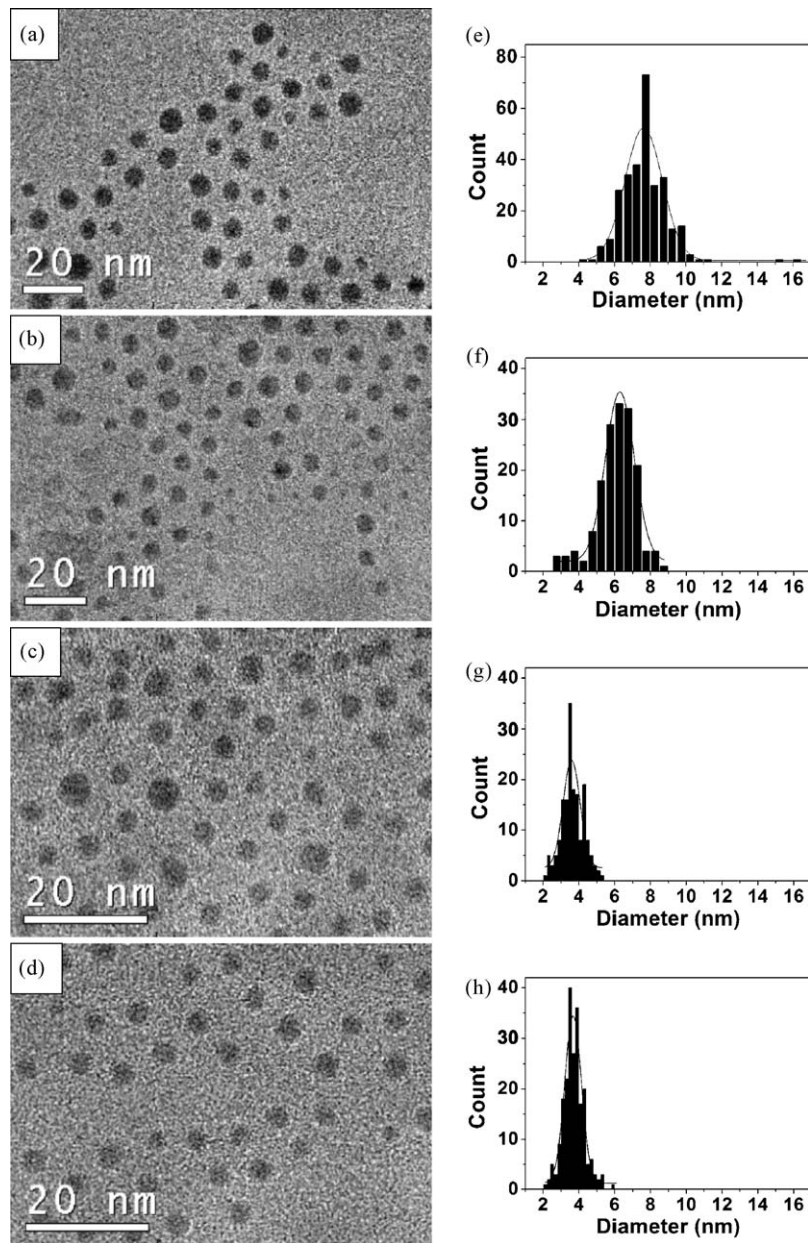


Fig. 1. TEM images of Co-NPs and corresponding size distributions: (a and e) 8Co-NPs-EtOH/SiO₂, (b and f) 6Co-NPs-EtOH/SiO₂, (c and g) 3Co-NPs-EtOH/SiO₂ and (d and h) 3Co-NPs-MeOH/SiO₂.

main reaction that takes place at low temperature:

$$\text{TOF}_n = \text{TOF}_f(1 - \eta) \quad (2)$$

$$\eta = \left(\frac{P_{\text{acetaldehyde}} \cdot P_{\text{H}_2}}{P_{\text{ethanol}}} \right) \left(\frac{1}{K_{\text{eq}}} \right) \quad (3)$$

where P is the partial pressure of each component and K_{eq} is the equilibrium constant. The difference between bulk and surface temperatures of ethanol and the difference in pressures are considered insignificant. The gas composition of reactants was analyzed by gas chromatography (Varian 3400 CX, equipped with two thermal conductivity detector with a Molecular Sieve and a W-chromosorb columns used in a parallel arrangement). The deposited carbon on catalysts with time on stream was calculated from carbon balance. The average rate of deposited carbon on used catalysts was determined by thermogravimetric analysis at the end of the reaction, using a SDT 2960 – TA Instruments.

3. Results and discussion

3.1. Synthesis and characterization

Co-NPs capped by OA were obtained by thermal decomposition of Co₂(CO)₈. OA/Co₂(CO)₈ molar ratios of 0.2, 0.4 and 0.8 were used to produce particles of different sizes, which were analyzed by TEM. The images and the corresponding histograms are shown in Fig. 1a–h, and the average diameters are presented in Table 1. The Co-NPs have spherical shape and narrow size distributions and by increasing the OA/Co₂(CO)₈ molar ratio, smaller nanoparticles were formed. This is expected since the OA binds to the particle surface, controlling the incorporation of new atoms and protecting against agglomeration; as a consequence, a larger excess of OA favors the formation of smaller nanoparticles [22]. Co-NPs synthesized with 0.8 OA/Co₂(CO)₈ molar ratio and precipitated with EtOH or MeOH showed similar average diameters of 3.6 ± 0.6 and 3.2 ± 0.6 (Table 1) in Fig. 1c, g and d, h, respectively.

Table 1

OA/Co₂(CO)₈ molar ratio used in the synthesis of the Co-NPs, Co content in the catalysts, average diameter of Co-NPs obtained by TEM, surface area (S_{BET}), H₂ uptake, TOF_f values and average rates of deposited carbon (r_{carbon}). The theoretical number of atoms per particle and the percentage of surface atoms are also shown.

| Samples | 8Co-NPs-EtOH/SiO ₂ | 6Co-NPs-EtOH/SiO ₂ | 3Co-NPs-EtOH/SiO ₂ | 3Co-NPs-MeOH/SiO ₂ |
|---|-------------------------------|-------------------------------|-------------------------------|-------------------------------|
| OA/Co ₂ (CO) ₈ (mol/mol) | 0.2 | 0.4 | 0.8 | 0.8 |
| Co (wt.%) | 9.1 | 9.8 | 9.4 | 9.6 |
| Co-NP size (nm) | 7.8 (± 1.3) | 6.1 (± 1.1) | 3.6 (± 0.6) | 3.2 (± 0.6) |
| S_{BET} ^a (m ² /g cat) | 40 | 54 | 81 | 79 |
| H ₂ uptake (μmol/g cat) | 60 | 64 | 32 | 82 |
| Number of atoms ^b | 62,070 | 29,689 | 6102 | 4286 |
| Surface atoms (%) | 10.1 | 12.9 | 21.9 | 24.6 |
| TOF _f (s ⁻¹) ^c | 0.002 | 0.038 | 0.024 | 0.055 |
| r_{carbon} (g h ⁻¹) ^d | 0.010 | 0.006 | 0.025 (0.002) ^e | 0.002 (0.002) ^e |

^a S_{BET} of SiO₂ support = 87 m²/g.

^b Estimate values considering the average size obtained by TEM.

^c TOF_f values calculated for dehydrogenation of ethanol at 580 K under steam reforming of ethanol (catalysts activated at 623 K and feed mixture of the 6:1 molar ratio of H₂O/ethanol).

^d Average rate of deposited carbon on catalysts activated at 623 K.

^e Activation at 773 K.

Fig. 2 (inset) presents a typical high resolution TEM (HRTEM) image of a Co-NP obtained by this colloidal synthesis, showing that they are crystalline. This was confirmed by XRD (Fig. 2, 8Co-NPs-EtOH/SiO₂ sample), which gives statistical signal. The XRD pattern matched to the ε-Co structure, with peaks at 46.9°, 49.5° and 52.0° corresponding to the reflections (2 2 1), (3 1 0) and (3 1 1), respectively [24]. The ε-Co is a metastable structure that has cubic symmetry and is usually obtained in the colloidal synthesis using Co₂(CO)₈ at high temperature.

Fig. 3 shows TEM images of the SiO₂-supported Co-NPs prepared in this work. The Co-NPs are well dispersed in the silica support and no agglomeration could be detected. Chemical analysis and surface area (S_{BET}) of the Co-NPs/SiO₂ catalysts are summarized in Table 1. All samples showed Co contents of about 9 wt.%. The SiO₂ support has a S_{BET} of 87 m²/g and the presence of Co-NPs led to a slight decrease of surface area, by partial agglomeration of SiO₂ particles. This effect was more pronounced when using smaller OA/Co₂(CO)₈ ratio.

One of the main challenges in exploring colloidal nanoparticles in catalysis is the presence of the capping layer [25–28]. While the ligands are essential to control the growth and protect the particles against agglomeration, they may also block the active sites for catalysis. A good compromise through the choice of the ligand or its removal by post-synthesis protocols is needed to make such samples catalytically active. Stowell and Korgel [27] showed that in the case of Ir nanoparticles, the best ligand for obtaining monodispersed nanoparticles also inhibited the activity for hydrogenation of decene. On the other hand, weaker ligands,

which resulted in nanoparticles with broader size distribution, led to good activity. In the case of Pt nanoparticles, Rioux et al. [28] showed that oxidation followed by reduction removed the polymer capping, increasing the performance in ethylene hydrogenation. Unfortunately, the use of a redox procedure in the case of Co on SiO₂ is not a good option. Co forms stable silicates when exposed to air and Co reduction is only achievable at very high temperatures (>800 K). In fact, this was one of the motivations for using already well-formed metallic Co-NPs instead of following the conventional methods, where Co salts are impregnated and then reduced. A fair amount of Co²⁺ always remains in these methods [23].

Our approach aimed to evaluate two effects: the solvent used to precipitate the Co-NPs (EtOH or MeOH) before impregnation and the temperature of the activation under H₂. Methanol is more aggressive to the Co-NPs and should remove the excess or weakly bonded ligand from the Co-NPs surface better than ethanol. Both effects were evaluated *in situ* by DRIFTS.

Fig. 4 shows the results of *in situ* DRIFTS measurements for 3Co-NPs-EtOH/SiO₂ and 3Co-NPs-MeOH/SiO₂ before and after activation under H₂ at 623 K. Both samples showed similar spectra and behavior. In a general way, the spectra presented bands at 2924 and 2854 cm⁻¹, characteristic of asymmetric and symmetric CH₂ stretch, respectively [26]. The weak band at 3005 cm⁻¹ could be assigned to the C–H stretch in C=C–H [26]. The characteristic band

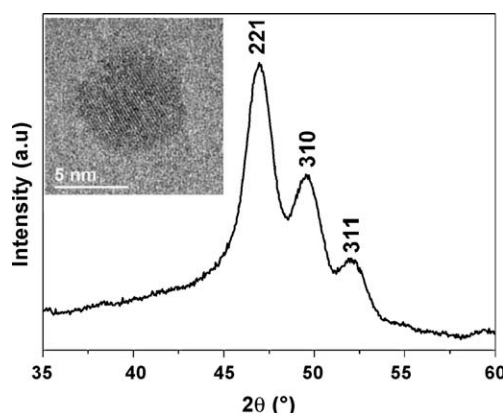


Fig. 2. XRD pattern of 8Co-NPs-EtOH/SiO₂ confirming the formation of ε-Co structure. (Inset) HRTEM image of a Co-NP showing lattice fringes with periodicity of 2.05 Å, corresponding to the (2 2 1) planes of the ε-Co.

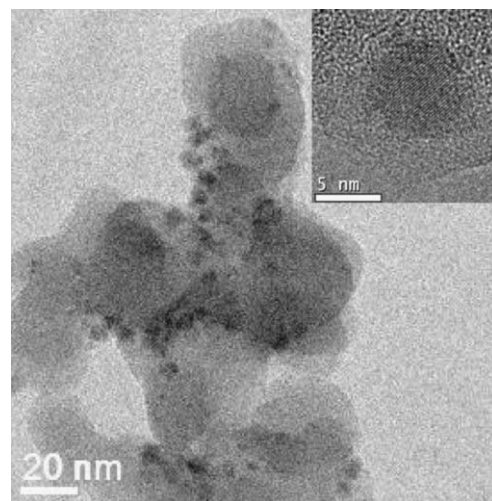


Fig. 3. TEM of 8Co-NPs-EtOH/SiO₂ catalyst. (Inset) HRTEM of Co-NP on the SiO₂ support.

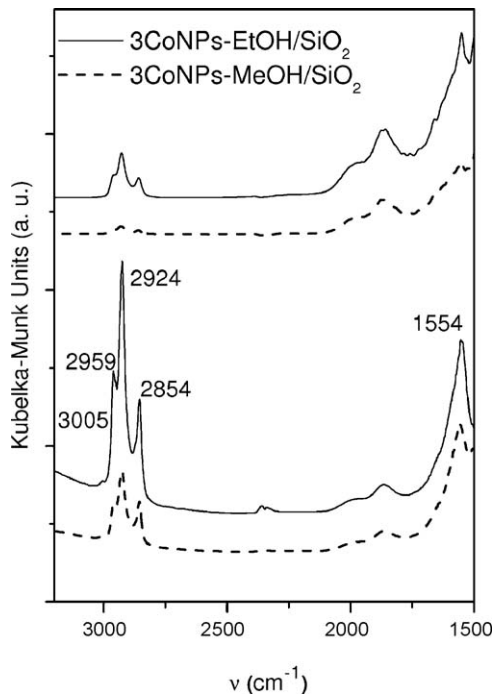


Fig. 4. FTIR measurements of the catalysts (—, 3Co-NPs-EtOH/SiO₂ and - - -, 3Co-NPs-MeOH/SiO₂) as prepared (bottom curves) and after heating under H₂ flow at 623 K (2 h) (top curves). All spectra were collected at 298 K.

of C=O of the carboxyl group at 1710 cm⁻¹, which appears in the spectrum of pure oleic acid [26], was absent in the spectra of Co-NPs/SiO₂ samples. This confirmed that the precipitation step succeeded in eliminating most of the free ligands. Nevertheless, a new band at 1554 cm⁻¹, assigned to asymmetric COO⁻ was present indicating that the OA molecules are chemisorbed as carboxylate on the Co-NP surface. When comparing the spectra of both samples activated at the same temperature, the precipitation with methanol led to a decrease in the intensity of the characteristic bands of OA. The bands at about 2959 and 1880 cm⁻¹ could not be easily identified. We tentatively attributed the band at 2959 cm⁻¹ to CH stretch in -CH₃ species formed by partial decomposition of the ligands.

The activation at 623 K significantly decreased the C-H stretch bands. However, residual OA was still present and the amount of organics was higher for Co-NPs precipitated with ethanol. This may explain the lower value in the hydrogen uptake obtained for the 3Co-NPs-EtOH/SiO₂ sample (Table 1). Additional DRIFTS measurements suggested that larger amount of OA remained when activation was performed at lower temperatures than 623 K and the complete removal of organics occurred only at 773 K (not shown). In the case of 8Co-NPs-EtOH/SiO₂ and 6Co-NPs-EtOH/SiO₂ catalysts, similar behavior was found but the band intensities were lower, reflecting the smaller amount of OA/Co used in the synthesis of larger Co-NPs. Interestingly, 8Co-NPs-EtOH/SiO₂ and 3Co-NPs-MeOH/SiO₂ catalysts activated at 623 K showed bands with similar intensities.

To further analyze the surface structure of the Co-NPs/SiO₂ catalysts, FTIR of adsorbed CO was obtained. Fig. 5a shows DRIFT results of Co-NPs/SiO₂ catalysts activated at 623 K; all spectra present the main band at about 2030 cm⁻¹ and a weak band at 2175 cm⁻¹. The spectra do not show an important contribution from the gaseous C=O stretching vibration. The asymmetry of the main band may indicate the presence of other components. According to the literature [29–31], the CO linearly bonded to Co²⁺ and Co³⁺ species shows a weak band in the 2160–2180 cm⁻¹ region and the band at 2175 cm⁻¹ corresponds to Co³⁺-CO species at high CO coverage [32]. The band in the 2075–2040 cm⁻¹ region is characteristic of linear carbonyl bonded to metallic Co, which shifts to about 2000 cm⁻¹ at zero coverage [29–32]. The band at ca. 2015 cm⁻¹ is characteristic of CO linearly bonded to one metallic Co site and the band in the 2060–2020 cm⁻¹ region is ascribed to different polycarbonyl Co(CO)_x ($x > 1$) species [29]. However, it is important to note that in our Co-NPs/SiO₂ catalysts the typical band of polycarbonyl species at about 1800–1700 cm⁻¹ was not observed. On the other hand, the CO linearly bonded to one metallic Co site in the presence of pre-adsorbed hydrogen shows a characteristic band at about 2050 cm⁻¹ assigned to the structure of hydrocarbonyl type [29,30].

Despite the similarities among all spectra, the intensities were remarkably different. The CO adsorption bands in the 1950–2070 cm⁻¹ region have higher intensity in the 6Co-NPs-EtOH/SiO₂ catalyst than in the 3Co-NPs-EtOH/SiO₂ one (Fig. 5a). The apparent disagreement with the smaller total surface area of the former can be understood when considering the higher amount of ligand attached to smaller particles [33]. These results could also be

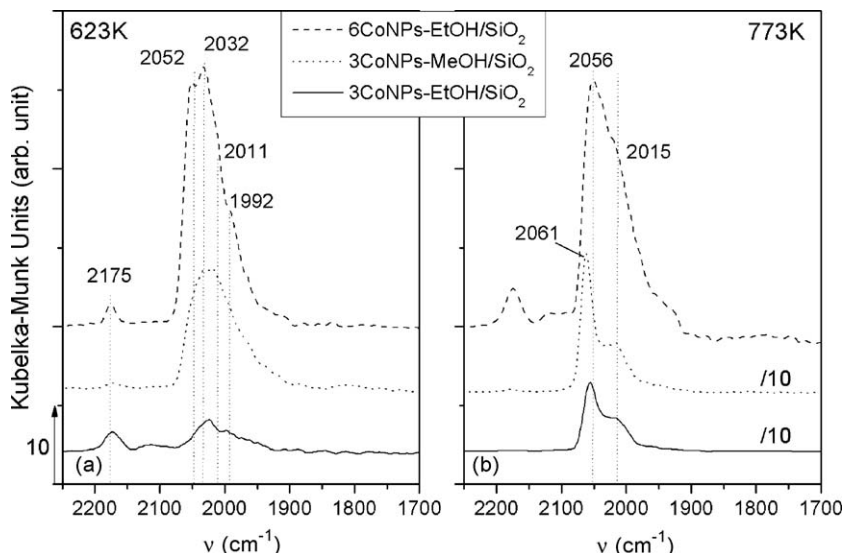


Fig. 5. FTIR-CO measurements of the catalysts after H₂ activation at (a) 623 K and (b) 773 K: - - -, 6Co-NPs-EtOH/SiO₂; · · ·, 3Co-NPs-MeOH/SiO₂; and —, 3Co-NPs-EtOH/SiO₂.

related to size dependent effects in which the adsorption of CO in hydrocarbon type on Co terrace sites would be favored in larger Co-NPs. Comparing the spectra of 3Co-NPs-EtOH/SiO₂ with 3Co-NPs-MeOH/SiO₂ catalysts in Fig. 5a, the latter shows adsorbed CO bands with higher intensity. These results are in agreement with DRIFTS measurements (Fig. 4), which indicated that a larger amount of OA was removed from Co-NPs during precipitation with MeOH.

Fig. 5b shows FTIR spectra of adsorbed CO of Co-NPs/SiO₂ catalysts activated at 773 K, where the main band at ca. 2060 cm⁻¹ and the shoulder at 2015 cm⁻¹ were now better resolved. In the case of 6Co-NPs-EtOH/SiO₂ catalyst, activation at either 623 or 773 K (Fig. 5a and b, respectively) led to CO bands with similar intensity. This suggests that in the case of large Co-NPs, synthesized with smaller amounts of OA, most of the ligand was already removed by activation at low temperature (623 K). On the other hand, a significant increase of CO adsorption in the case of the smaller Co-NPs (3Co-NPs-EtOH/SiO₂ and 3Co-NPs-EtOH/SiO₂ catalysts) was detected by increasing the activation temperature to 773 K (note the divider factors in Fig. 5b). As a result, a more stringent treatment was required to expose a larger number of Co sites in smaller NPs. The best result was found for 3Co-NPs-MeOH/SiO₂ that combined a more effective removal of free and weakly bonded ligand in the precipitation step and the removal of remaining ligand at higher temperature. It is interesting to note that these results are different from the one obtained by Saib et al. [34] using the impregnation technique, where the treatment at high temperature led to the encapsulation of the Co-NPs by a silica shell.

3.2. Hydrogenolysis and steam reforming of ethanol

The steam reforming of ethanol (Eq. (1)) is a complex reaction [35], which involves the adsorption of ethanol on the catalyst surface with dehydrogenation and rupture of C–C bond, resulting in two radicals with different reactivities for oxidation by H₂O to produce H₂ and CO₂. Haga et al. [14] suggested that steam reforming on Co based catalysts occurs directly without going through methane formation. On the other hand, Frusteri et al. [36] suggested that ethanol is decomposed into products such as methane and CO, which then react to produce CO₂ and H₂. Methane would be formed if the decomposition of ethanol takes place, according to Eq. (4), or through methanation. The hydrogenolysis of ethanol is favored at low H₂O:ethanol molar ratio and low temperatures [37] and it has been proposed [38] that it occurs through dehydrogenation of ethanol forming acetaldehyde followed by decomposition, according to Eqs. (5) and (6).



In fact, complex reaction pathways may be involved in the steam reforming of ethanol depending on the reaction conditions [37]. Water-gas shift reaction (Eq. (7)) and steam reforming of methane (Eq. (8)) could also take place and would convert CO and CH₄ to the desired product, H₂. The formation of methane, however, hinders the formation of H₂ since the steam reforming of methane occurs at higher temperature than the steam reforming of ethanol [39,40].

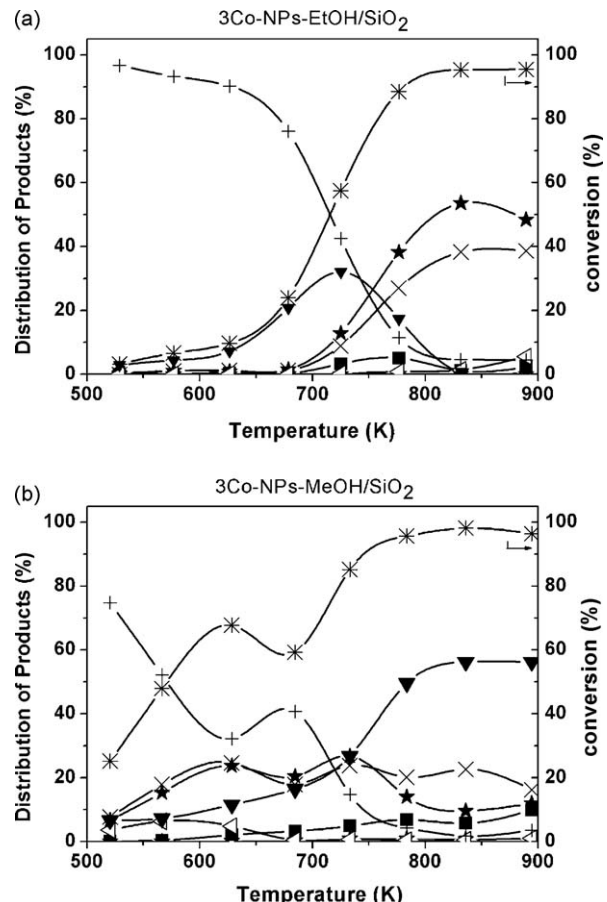


Fig. 6. Distribution of products and ethanol conversion for hydrogenolysis of ethanol on Co-NPs/SiO₂ catalysts after H₂ activation at 623 K: (a) 3Co-NPs-EtOH/SiO₂ and (b) 3Co-NPs-MeOH/SiO₂. Symbols: ★, CO; ×, CH₄; ■, ethylene; ▼, acetaldehyde; ▲, methanol; +, ethanol and * ethanol conversion ($w_{\text{cat}} = 160$ mg and H₂/ethanol molar ratio = 3).

Another undesired reaction is the formation of ethylene by the dehydration of ethanol, but it requires acid sites, usually related to the support properties (Eq. (9)).



To understand the catalytic properties of Co-NPs/SiO₂ catalysts in the steam reforming of ethanol, we initially evaluated the hydrogenolysis of ethanol. Rostrup-Nielsen and Alstrup [41] showed that the rates of steam reforming and hydrogenolysis are closely correlated indicating common rate controlling steps in the case of ethane.

Fig. 6a and b shows the product distribution and ethanol conversion in the hydrogenolysis of ethanol when using 3Co-NPs-EtOH/SiO₂ and 3Co-NPs-MeOH/SiO₂ catalysts activated at 623 K. These catalysts have similar Co-NP sizes that are the smaller ones within the Co-NPs/SiO₂ series investigated here (Table 1).

In the case of 3Co-NPs-EtOH/SiO₂ catalyst (Fig. 6a), the ethanol was mainly dehydrogenated to acetaldehyde (Eq. (5)) at low temperature (<700 K). At about 680 K, it began the formation of CH₄ and CO while maximum formation of acetaldehyde was achieved at 720 K. These results suggest that ethanol decomposed on Co surface via adsorbed acetaldehyde; the intermediate surface CH_x–CHO species were cracked to form (a) –CH_x(ads) species, which were hydrogenated to form CH₄, and (b) carbon–oxygen – CHO(ads) species, which led to the formation of CO (Eq. (4)). These results are similar to the one observed for decomposition of ethanol on Ni surfaces [35]. Considering that CH₄/CO molar ratio

was lower than 1, it is possible that during the dissociative adsorption of ethanol a fraction of $-\text{CH}_x$ species irreversibly attached to the Co surface. These species would evolve to carbonaceous compounds on Co surface by $-\text{CH}_x$ condensation and/or successive abstraction of hydrogen. The ethanol conversion to ethylene began at 680 K but was small, indicating the presence of weak acid sites on the catalyst. In this sample, FTIR of adsorbed CO pointed out the presence of small amounts of Co^{2+} (indicated by the band at 2175 cm^{-1} in Fig. 5a) and the presence of acid sites is probably related to the formation of cobalt silicates. This is in agreement with studies realized by Kaddouri and Mazzocchia [19] that showed a strong interaction between cobalt ions and silica, leading to the formation of silicates and/or hydrosilicates. In our case, however, the impregnation of already formed metallic Co-

NPs prevented this interaction and the amount of ethylene that was formed was very small.

Interestingly, 3Co-NPs-MeOH/SiO₂ catalyst (Fig. 6b) began to form CH₄ and CO at temperatures about 200 K lower than in the case of 3Co-NPs-EtOH/SiO₂ catalyst. CH₄ and CO were also produced in larger amounts than acetaldehyde at this temperature by the 3Co-NPs-MeOH/SiO₂ catalyst. Although the Co-NPs in both catalysts have similar sizes, the FTIR of adsorbed CO and H₂ uptake indicated that the former has a larger number of exposed Co sites. These results suggest that the residual ligand may have partially suppressed Co sites that were active for adsorption of acetaldehyde and cleavage of C–C bond to form CH₄ and CO. The 3Co-NPs-MeOH/SiO₂ catalyst also showed a decrease of ethanol conversion at temperature about 680 K, which is probably associated to strong

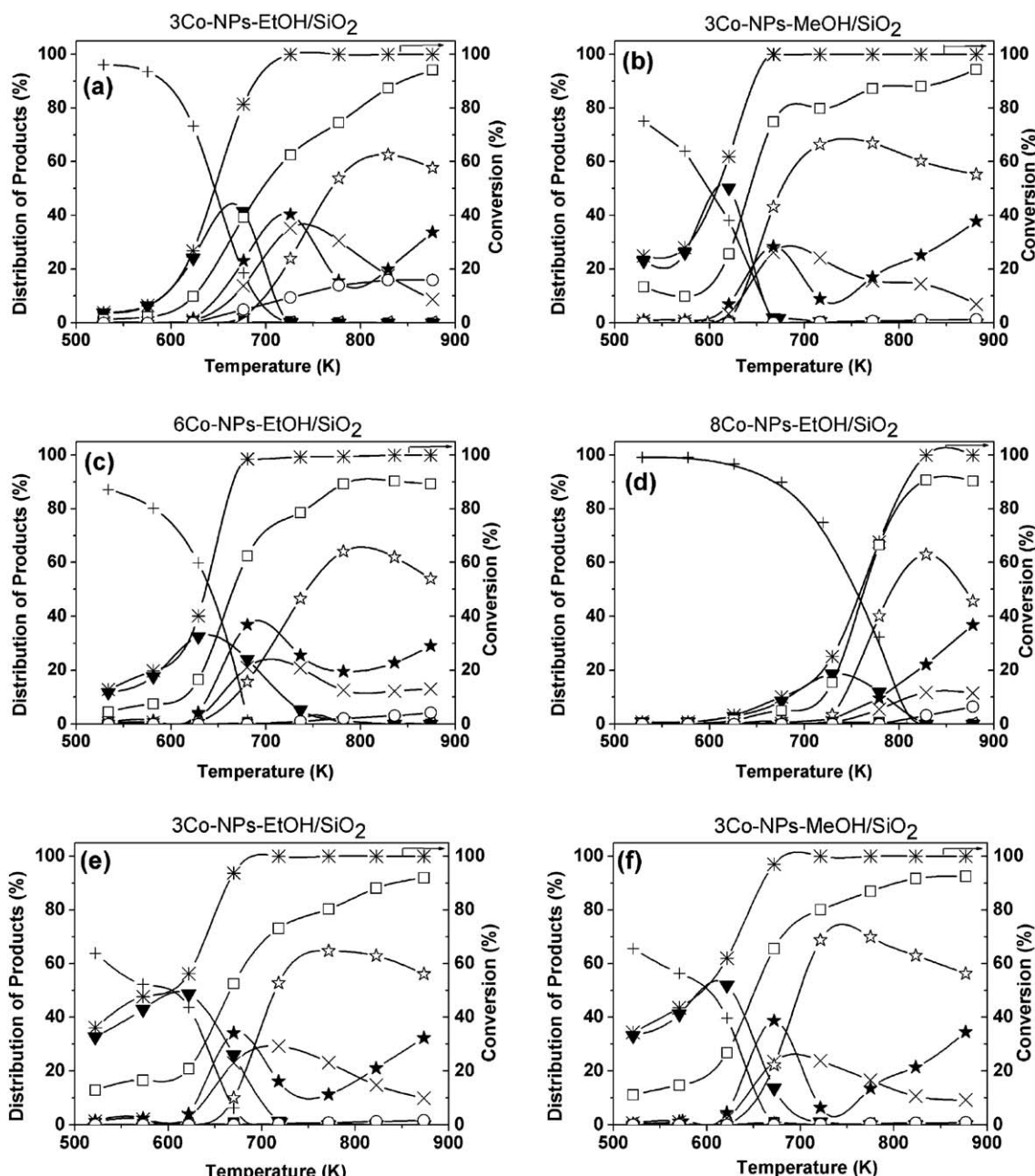


Fig. 7. Distribution of products and ethanol conversion for steam reforming of ethanol on Co-NPs/SiO₂ catalysts after H₂ activation at 623 K: (a) 3Co-NPs-EtOH/SiO₂, (b) 3Co-NPs-MeOH/SiO₂, (c) 6Co-NPs-EtOH/SiO₂, and (d) 8Co-NPs-EtOH/SiO₂. H₂ activation at 773 K: (e) 3Co-NPs-EtOH/SiO₂ and (f) 3Co-NPs-MeOH/SiO₂. Symbols: ★, CO; ×, CH₄; ▲, CO₂; ■, ethylene; ▽, acetaldehyde; +, ethanol; □, H₂; ○, deposited carbon and * ethanol conversion ($w_{\text{cat}} = 160\text{ mg}$ and $\text{H}_2/\text{ethanol} = 6$).

adsorption of products during the decomposition of intermediates on C-C cleavage.

Fig. 7 presents the results for the steam reforming of ethanol. A strong dependence on the Co-NP size (**Fig. 7a, c and d**), solvent used to precipitate the Co-NPs (**Fig. 7a and b**), and activation temperature under H₂ flow (**Fig. 7a, e and b, f**) was verified.

For samples activated at 623 K (**Fig. 7a-d**), the results pointed out that at low temperatures ($T < 650$ K), the ethanol was mainly dehydrogenated to acetaldehyde (Eq. (5)) and **Table 1** gives the TOF_f values calculated at 580 K. Compared to the hydrogenolysis experiments (**Fig. 6**), the decomposition of acetaldehyde was strongly suppressed by the presence of H₂O. For Co-NPs precipitated with EtOH, the TOF_f values increased as: 8Co-NPs-EtOH/SiO₂ < 3Co-NPs-EtOH/SiO₂ < 6Co-NPs-EtOH/SiO₂. The smaller TOF_f value of 3Co-NPs-EtOH/SiO₂ compared to 6Co-NPs-EtOH/SiO₂ can be explained by the low accessibility of Co sites, as shown by the H₂ uptake and FTIR of adsorbed CO. In the case of 3Co-NPs-MeOH/SiO₂ catalyst, the better removal of ligand is in agreement with its highest TOF_f value. On the other hand, 8Co-NPs-EtOH/SiO₂ catalyst has low ligand coverage but still showed a very low TOF_f value, suggesting that a size dependent effect might compete.

The distribution of products when increasing the temperature shows that the decomposition of acetaldehyde took place (Eq. (6)) producing CH₄ and CO. Comparing 8Co-NPs-EtOH/SiO₂ (**Fig. 7d**) and 3Co-NPs-MeOH/SiO₂ (**Fig. 7b**) samples, both with low coverage by ligands, the temperature in which the acetaldehyde began to decompose forming CH₄ and CO was about 100 K higher for the former. These results point out that the decomposition of acetaldehyde was strongly favored by decreasing the Co-NP size. From DFT calculations, Gong et al. [42,43] showed that the barriers of the elementary step for CH₃ hydrogenation on both flat and stepped surfaces are similar, with similar energy profiles. Therefore, it has been proposed that the -CH_x hydrogenation is not structure-sensitive. In this framework and based on our experimental results, the decrease of Co-NP size led to more Co sites that favored C-C bond cleavage, required to the formation of CH₄ and CO.

At higher temperature, CO₂ was also formed and the maximum formation of CO and CH₄ took place near the total ethanol conversion, for all catalysts. The exception was 8Co-NPs-EtOH/SiO₂ where the total ethanol conversion occurred only at very high temperature (>800 K). In this case, other reactions, such as the reverse water-gas shift reaction, also affected the distribution of products.

More interesting, the (CO + CO₂)/CH₄ molar ratio was much higher than 1 before achieving total ethanol conversion. This is direct evidence that ethanol could be reformed in one step on Co surface, where CO₂ (and H₂) were formed by activation of H₂O and oxidation of radicals -CH_x and -CHO, originated from cleavage of C-C bond of adsorbed CH_x-CHO species.

It is worth noting that the temperature in which CO₂ began to be formed in the case of 3Co-NPs-MeOH/SiO₂ catalyst (and as a consequence H₂O was activated) was also about 100 K lower than in the case of 8Co-NPs-EtOH/SiO₂ catalyst (**Fig. 7b and d**). It is well established that the average coordination numbers of metal decrease with decreasing of metal nanoparticle size. As demonstrated by DFT calculations, the activation of H₂O on metal surfaces is sensitive to structure of metal [44] and that stepped surfaces have lower barriers to the reaction than planar surfaces. Our results are in agreement with these calculations, suggesting that the activation of H₂O was favored for smaller Co-NP sizes due to the larger number of metal sites with low coordination.

Fig. 7e and f shows the results when 3Co-NPs-EtOH/SiO₂ and 3Co-NPs-MeOH/SiO₂ catalysts were activated at 773 K. A careful analysis showed that the catalysts activated at 773 K presented comparable ethanol conversion to 3Co-NPs-MeOH/SiO₂ catalyst activated at 623 K, confirming that both the solvent used to precipitate the Co-NPs and the activation temperature were important to achieve high accessibility to Co sites. Comparing the performances of both 3Co-NPs-EtOH/SiO₂ catalysts (**Fig. 7a and e**), the temperature in which CO₂ began to form was lower for the activation at 773 K and the maximum of CH₄ production decreased from about 40% to 30%. These results suggest that residual OA on Co-NP surface blocked the most active Co sites for H₂O activation,

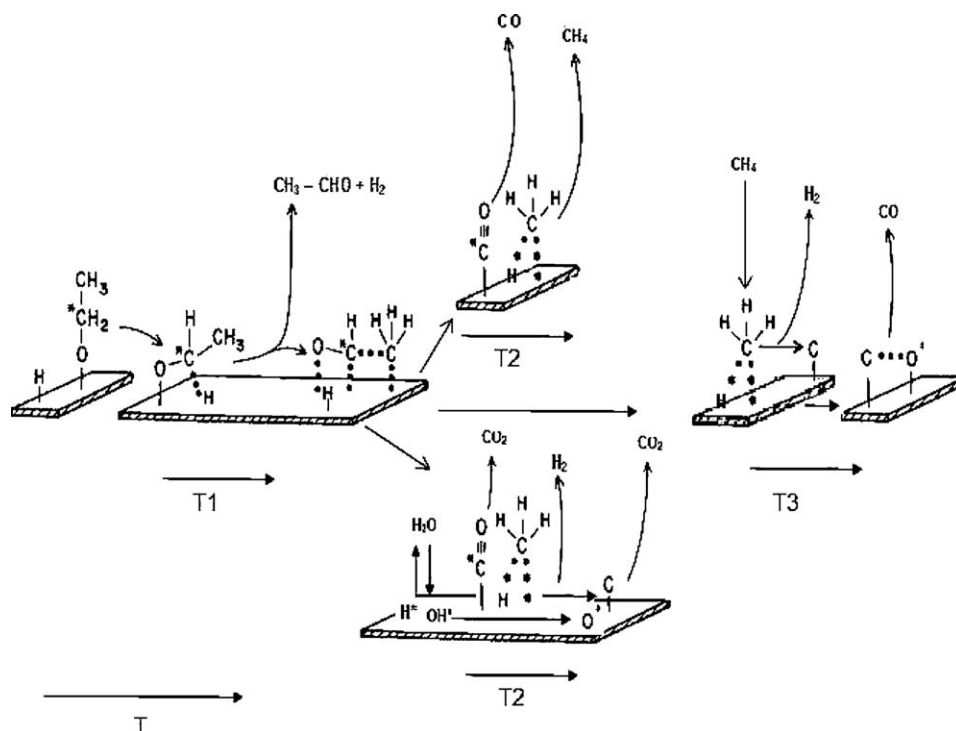


Fig. 8. Scheme for ethanol reactions in the presence of H₂O on Co-NPs surfaces with increasing temperatures, T .

which would lead to the oxidation of radicals formed by activation and cleavage of C–C bond intermediates. This explains the larger carbon deposition on 3Co-NPs-EtOH/SiO₂ (Table 1).

From designing Co-NPs/SiO₂ catalysts with different Co-NP sizes and based on the distribution of products with the temperature of reaction, it is likely that H₂ could be formed from steam reforming of ethanol by different reaction pathways (Fig. 8):

- (1) Adsorption of ethanol and dehydrogenation forming CH_x–CHO intermediate surface species, with acetaldehyde and H₂ desorbing at low temperature range, T₁.
- (2) Cleavage of the CH_x–CHO intermediate surface species forming –CH_x(ads) and –CO(ads) at medium temperature range, T₂. Two reactions pathways may take place: (a) hydrogenation/dehydrogenation of –CH_x(ads) and –CO(ads) resulting in desorption of CH₄ and CO (“hydrogenolysis step”), and (b) chemisorption and decomposition of H₂O to H* and OH* in parallel to the decomposition of –CH_x(ads) to C(ads) and H₂(g), and oxidation of C(ads) and CO(ads) by O* forming CO₂(g) (“steam reforming step”).
- (3) Activation of CH₄ for steam reforming through C(ads) and oxidation to CO and CO₂ by H₂O (Eqs. (5) and (6)), at T₃.

4. Conclusions

Co-NP/SiO₂ catalysts obtained from narrow size distribution colloidal NPs were successfully produced and their performances in steam reforming of ethanol were analyzed. The number of accessible Co sites to ethanol strongly depended on the NP synthesis conditions such as the OA/Co₂(CO)₈ ratio, solvent used to precipitate the Co-NPs and the activation temperature.

The use of colloidal Co-NPs to produce model catalysts for steam reforming of ethanol has shown a promising approach to address in detail aspects that are related to the reaction pathways. The selectivity dependence on the Co-NP size was shown, with smaller Co-NPs favoring the hydrogenolysis of ethanol and activation of H₂O. A mechanism for the steam reforming of ethanol was suggested based on the distribution of products with temperature and the detailed characterization of the catalysts.

Specific issues related to the use of Co colloidal nanoparticles in catalysis were also evaluated and we hope that these results will contribute to the development of new strategies to improve catalysts, such as the right balance between capping and catalytic performance and exploitation of the anchorage properties of the supports and ligands.

Acknowledgments

The authors are grateful for the financial support of CNPq (Conselho Nacional de Desenvolvimento Científico e Tecnológico), FINEP (Financiadora de Estudos e Projetos) and FAPESP (Fundação de Apoio à Pesquisa do Estado de São Paulo). We thank LNLS for the access of XRD2 beamline and TEM (LME). T.C.R. Rocha, C.B. Rodella,

S.B. Betim and F.R. Zambello are acknowledged for their support during sample preparation, H₂ chemisorption and XRD measurements. H.W. acknowledges FAPESP for the fellowship.

References

- [1] G.A. Somorjai, T. Feng, J.Y. Park, Top. Catal. 47 (2008) 1.
- [2] R. Schlägl, S.B.A. Hamid, Angew. Chem. Int. Ed. 43 (2004) 1628.
- [3] S.H. Wu, D.H. Chen, J. Colloid Interface Sci. 259 (2003) 282.
- [4] Z. Kónya, V.F. Puntes, I. Kiricsi, J. Zhu, P. Alivisatos, G.A. Somorjai, Catal. Lett. 81 (2002) 137.
- [5] E. Barea, X. Batlle, P. Bourges, A. Corma, V. Fornés, A. Labarta, V.F. Puntes, J. Am. Chem. Soc. 127 (2005) 18026.
- [6] G.A. Somorjai, J.Y. Park, J. Chem. Phys. 128 (2008) 182504.
- [7] R. Narayanan, M.A. El-Sayed, Langmuir 21 (2005) 2027.
- [8] R.M. Rioux, H. Song, J.D. Hoefelmeyer, P. Yang, G.A. Somorjai, J. Phys. Chem. B 109 (2005) 2192.
- [9] R. Narayanan, M.A. El-Sayed, J. Am. Chem. Soc. 126 (2004) 7194.
- [10] R. Narayanan, M.A. El-Sayed, Nano Lett. 4 (2004) 1343.
- [11] H. Song, R.M. Rioux, J.D. Hoefelmeyer, R. Komor, K. Niesz, M. Grass, P. Yang, G.A. Somorjai, J. Am. Chem. Soc. 128 (2006) 3027.
- [12] S. Cavallaro, N. Mondello, S. Freni, J. Power Sources 102 (2001) 198.
- [13] T. Ioannides, J. Power Sources 92 (2001) 17.
- [14] F. Haga, T. Nakajima, H. Miya, S. Mishima, Catal. Lett. 48 (1997) 223.
- [15] A.N. Fatsikostas, D.I. Kondarides, X.E. Verykios, Chem. Commun. (2001) 851.
- [16] J. Llorca, N. Hom, J. Sales, P. Ramires de la Piscina, J. Catal. 209 (2002) 306.
- [17] F. Haga, T. Nakajima, K. Yamashita, S. Mishima, React. Kinet. Catal. Lett. 63 (1998) 253.
- [18] H. Song, L. Zhang, R.B. Watson, D. Braden, U.S. Ozkan, Catal. Today 129 (2007) 346.
- [19] A. Kaddouri, C. Mazzocchia, Catal. Commun. 5 (2004) 339.
- [20] J. Llorca, P. Ramires de la Piscina, J.A. Dalmon, J. Sales, N. Hom, Appl. Catal. B: Environ. 43 (2003) 355.
- [21] H. Song, U.S. Ozkan, J. Catal. 261 (2009) 66.
- [22] V.F. Puntes, K.M. Krishnan, A.P. Alivisatos, Science 291 (2001) 2115.
- [23] E.L. Rodrigues, J.M.C. Bueno, Appl. Catal. A: Gen. 232 (2002) 147.
- [24] S. Sun, C.B. Murray, J. Appl. Phys. 85 (1999) 4325.
- [25] R. Rinaldi, A.M. Porcari, T.C.R. Rocha, W.H. Cassinelli, R.U. Ribeiro, J.M.C. Bueno, D. Zanchet, J. Mol. Catal. A: Chem. 301 (2009) 11.
- [26] N.Q. Wu, L. Fu, M. Su, M. Islam, K.C. Wong, V.P. Dravid, Nano Lett. 4 (2004) 383.
- [27] C.A. Stowell, B.A. Korgel, Nano Lett. 5 (2005) 1203.
- [28] R.M. Rioux, H. Song, M. Grass, S. Habas, K. Niesz, J.D. Hoefelmeyer, P. Yang, G.A. Somorjai, Top. Catal. 39 (2006) 167.
- [29] M.J. Heal, E.C. Leiseigang, R.G. Torington, J. Catal. 51 (1978) 314.
- [30] G. Kadinov, Ch. Bonev, S. Todorova, A. Palazov, J. Chem. Soc., Faraday Trans. 94 (1998) 3027.
- [31] A. Lapidus, A. Krylova, V. Kazanskii, V. Borovkov, A. Zaitseu, J. Rathousky, A. Zukal, M. Jancáková, Appl. Catal. 73 (1991) 65.
- [32] A. Yu Khodakov, J. Lynch, D. Bazin, B. Rebours, N. Zanier, B. Moisson, P. Chaumette, J. Catal. 168 (1997) 16.
- [33] B.A. Korgel, S. Fullam, S. Connolly, D. Fitzmaurice, J. Phys. Chem. B 102 (1998) 8379.
- [34] A.M. Saib, A. Borgna, J. van de Loosdrecht, P.J. van Berge, J.W. Geus, J.W. Niemannsverdriet, J. Catal. 239 (2006) 326.
- [35] J.W.C. Liberatori, R.U. Ribeiro, D. Zanchet, F.B. Noronha, J.M.C. Bueno, Appl. Catal. A: Gen. 327 (2007) 197.
- [36] F. Frusteri, S. Freni, L. Spadaro, V. Chiodo, G. Bonura, S. Donato, S. Cavallaro, Catal. Commun. 5 (2004) 611.
- [37] I. Fishlik, A. Alexander, R. Datta, D. Geana, Int. J. Hydrogen Energy 25 (2000) 31.
- [38] A. Haryanto, S. Fernando, N. Murali, S. Adhikari, Energy Fuels 19 (2005) 2098.
- [39] S. Cavallaro, V. Chiodo, S. Freni, N. Mondello, F. Furteri, Appl. Catal. A: Gen. 249 (2003) 229.
- [40] K. Vasudeva, N. Mitra, P. Umasankar, S.C. Dhingra, Int. J. Hydrogen Energy 21 (1996) 13.
- [41] J.R. Rostrup-Nielsen, I. Alstrup, Catal. Today 53 (1999) 311.
- [42] X.-Q. Gong, R. Raval, P. Hu, J. Chem. Phys. 122 (2005) 24711.
- [43] J. Cheng, X.-Q. Gong, P. Hu, C.M. Lok, P. Ellis, S. French, J. Catal. 254 (2008) 285.
- [44] H.S. Bengaard, J.K. Nørskov, J. Sehested, B.S. Clausen, L.P. Nielsen, A.M. Molenbroek, J.R. Rostrup-Nielsen, J. Catal. 209 (2002) 365.